A Wearable Microwave Antenna Array for Time-Domain Breast Tumor Screening

Emily Porter, Hadi Bahrami, Adam Santorelli, Benoit Gosselin, Leslie A. Rusch, and Milica Popović

A Wearable Microwave Antenna Array for Time-Domain Breast Tumor Screening

E. Porter, *Student Member, IEEE*, H. Bahrami, *Student Member, IEEE*, A. Santorelli, *Student Member, IEEE*, B. Gosselin, *Member, IEEE*, L. A. Rusch, *Fellow, IEEE*, and M. Popović, *Senior Member, IEEE*

Abstract—In this work, we present a clinical prototype with a wearable patient interface for microwave breast cancer detection. The long-term aim of the prototype is a breast health monitoring application. The system operates using multistatic time-domain pulsed radar, with 16 flexible antennas embedded into a bra. Unlike the previously reported, table-based prototype with a rigid cup-like holder, the wearable one requires no immersion medium and enables simple localization of breast surface. In comparison with the table-based prototype, the wearable one is also significantly more cost-effective and has a smaller footprint. To demonstrate the improved functionality of the wearable prototype, we here report the outcome of daily testing of the new, wearable prototype on a healthy volunteer over a 28-day period. The resulting data (both signals and reconstructed images) is compared to that obtained with our table-based prototype. We show that the use of the wearable prototype has improved the quality of collected volunteer data by every investigated measure. This work demonstrates the proof-of-concept for a wearable breast health monitoring array, which can be further optimized in the future for use with patients with various breast sizes and tissue densities.

Index Terms—Biomedical monitoring, Breast cancer detection, Flexible antennas, Microwave antenna arrays, Multistatic radar.

I. INTRODUCTION

MICROWAVE imaging techniques have been proposed as a complementary modality to the standard x-ray mammography for breast cancer screening and detection. Based on an inherent contrast in the dielectric properties of healthy and malignant breast tissues [1], microwave methods have the potential to discriminate between cancerous growths and healthy or benign tissues. Unlike mammography,

microwave techniques do not use ionizing radiation [2] and thus breast scans can safely be performed frequently, making them excellent candidates for diagnostic breast screening.

Microwave techniques are typically categorized into two subtypes: microwave radar and microwave tomography. These techniques can be performed with physical measurements in either the time or the frequency domain. Time-domain recordings allow collection of data over a wide frequency band with one pulse, allowing for potentially faster recordings; however, they suffer from poorer signal to noise ratios (SNR) than frequency domain methods [3].

In recent research on microwave breast cancer detection, multiple experimental systems have evolved to the stage of clinical measurements. Such studies involve performing breast scans on women, either healthy volunteers or those who have been diagnosed with breast cancer [4] – [7]. For each of these studies, the patient was positioned prone on a bed or table during the breast scan.

Microwave techniques are particularly promising for monitoring applications, wherein conventional methods fall short. There are two main monitoring applications: healthy patient screening for timely detection of cancerous growths, and post-diagnosis treatment progress tracking for patients with cancer. Mammography is not often used for monitoring due to the ionizing radiation and associated health risks, whereas magnetic resonance imaging (MRI) or positron emission tomography (PET) technologies are expensive and not sufficiently accessible [8]. Microwave monitoring of the breast has been investigated in [8], where a series of eight women were followed with breast scans post-diagnosis throughout their treatment course. In particular, each had breast scans taken between five and eight times from the time of tumor diagnosis until either the end of the treatment cycle or the study, with a table-based tomography system. The work demonstrated that dielectric property changes correlated with the tissue response during treatment, demonstrating the promise for such monitoring technologies in practice.

In our work, we use a time-domain radar system for breast health monitoring. The long-term aim of the research is a device for breast monitoring as an early warning indicator for cancer that uses several metrics to assess breast health. Such an application would be of particular use with patients who are at high risk of developing breast cancer. The envisioned device would allow the recording of several metrics, for which

patient scans over time would provide a healthy baseline range of values. If future scans result in values that deviate from the expected healthy range, it could indicate that there are suspicious tissue changes occurring, and further investigation would be necessary.

In previous studies, we have presented an initial clinical prototype for feasibility tests [9], [10]. This table-based prototype was composed of a radome with embedded antennas. During a scan, patients lay on the table in the prone position with their breast in the radome. Using the table-based prototype, we performed breast scans on a volunteer daily over the course of one month [10]. This study helped identify avenues towards an improved prototype. Namely, we now aim to develop a prototype that does not require the table setup, thus making it more portable and compact. A more cost-effective solution is also beneficial, in order to enable wider accessibility.

In this work, we introduce a second-generation prototype that is advanced with respect to the initial device in the above-mentioned ways. First, this prototype has a wearable patient interface, with no need for the patient exam table. Thus, the wearable prototype has a significantly smaller footprint than the table-based one, and is more cost-effective. Second, unlike its predecessor, the new, here-presented wearable prototype does not require immersion medium and, due to a close fit with the fabric hosting the antenna-array, the position of the breast relative to the array is known. This eliminates the effect of errors in imaging caused by the immersion, and reduces uncertainties in breast positioning. In this study, breast scans are performed regularly using the wearable prototype on a healthy volunteer in a breast-monitoring context. Through the daily measurements, we demonstrate the improved functionality of the wearable prototype, with planar, broadside-radiating antennas. These results demonstrate that the wearable prototype has achieved the goal of a more compact, cost-effective system, while simultaneously improving the quality of data collected.

The following section offers the details of the radar system operation. We also provide an overview of the table-based prototype and its associated challenges, and then introduce the wearable prototype. In Section III, interfacing with the volunteer is described along with the measurement parameters. Previously performed measurements with the table-based prototype are summarized as they will be used in this work for comparison, then measurements with the wearable prototype are discussed. Section IV presents signal data and related results, while Section V details imaging analysis and results. Finally, Section VI provides a summary and conclusion for the presented study.

II.   PROTOTYPE DESCRIPTIONS

This section describes the time-domain microwave radar system operation for breast cancer detection. The table-based prototype, presented in past work [9], is summarized for reference and comparison, while the new wearable prototype is the focus of this work. The prototypes differ in terms of the patient interface (antennas, array, and the array-holding

structure), while the rest of the hardware components remain unchanged. Both prototypes operate on the same principle, which is detailed first in the following subsection. Then, the table-based prototype is overviewed, along with a discussion of the related drawbacks and deficiencies. Finally, a description of the new, wearable prototype is provided.

A.   General System Operation

The system operates based on the multistatic radar principle. A short-duration pulse (with frequency content in the 2-4 GHz range) is generated on each clock cycle. It is then amplified and transmitted, through a switching matrix, to a transmitting antenna. The system is composed of a 16-element wideband antenna array, which surrounds the breast under test.

The wave propagates through the breast tissues, scattering at each interface of different tissue types. The resulting scattered wave is collected at each of the 15 receiving antennas in turn. An equivalent-time sampling oscilloscope ('picoscope') is used to record the data, which is stored digitally. The switching matrix then changes the transmitting antenna, and the recording process is repeated until all possibilities have been cycled through. A total of 240 multistatic signals constitute a complete breast scan. A schematic of the measurement setup is provided in Fig. 1.
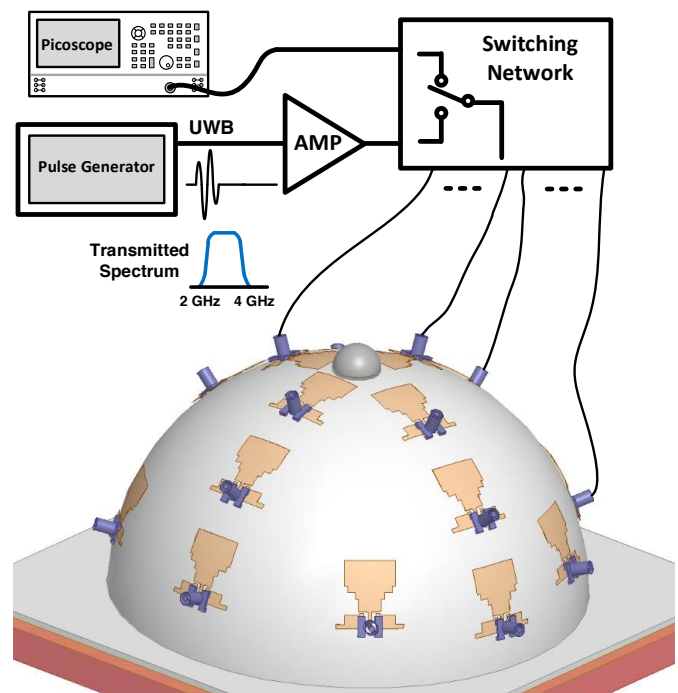
Fig. 1. Schematic drawing of the microwave radar system: A pulse is generated and amplified (AMP), then fed into a switching network which selects the transmitting and receiving antennas. The antennas are positioned surrounding the breast. The received signal is recorded by a picoscope. The drawing shows only select antenna connections for clarity.

B.   Overview of Table-Based Prototype

The table-based prototype was presented in detail in [9]. For clinical testing, the radome and antenna array were positioned in a table along with the measurement equipment. In order for

the prototype to fit women with various breast sizes, the radome was designed to accommodate the largest anticipated size. An immersion medium of ultrasound gel (measured relative permittivity ε_r = 68, conductivity σ = 3 S/m, at the centre frequency of 3 GHz) was used for smaller breasts, to avoid air gaps.

While this initial prototype was a suitable first step in testing with volunteers, many lessons were learned from its shortcomings. The antennas were delicate to fabricate and thus costly. Further, with end-fire radiation [11], they had to be held perpendicular to the tangent of the breast surface for optimal microwave illumination. Due to this required orientation with respect to the breast, a thick, sturdy radome was needed to secure the antennas. With the size and shape of the radome, as mentioned above, use of an immersion medium was unavoidable. While the lossy ultrasound gel attenuated the reverberating reflections between the radome walls and the breast skin, it also lowered the received signal amplitude and added reflection interfaces along the signal path. Further, use of the immersion medium also made the position of the breast surface relative to the hemispherical radome walls (and, thus, the array) difficult to estimate.

C. Upgraded Prototype with Wearable Array

The wearable prototype presented in this work aims to overcome the challenges associated with the table-based prototype, as discussed in the previous subsection.

The wearable prototype uses flexible monopole antennas, the design of which is detailed in [12] and overviewed in [13]. The antennas are designed specifically for this application, and are intended to contact the skin directly. This eliminates the need for an immersion medium, and further allows for precise knowledge of the skin relative to the antennas (as they are touching). Through simulation of the antenna and initial test measurements on tissue-mimicking phantoms, we demonstrated that the reflection coefficient (S_{11}) and transmission coefficient (S_{21}) characteristics are acceptable over our frequency range of interest [12] (i.e.,. S_{11} < - 10 dB, and S_{21} in the expected range given path length and tissue losses). The radiation for this monopole antenna is not end-fire, but broadside [12]. This difference in radiation pattern allows the wearable prototype, where the antennas are now tangential to the skin surface, to eliminate the need for the ceramic radome that held the antennas perpendicularly to the breast surface in the table-based prototype.

In this work, a wearable prototype is fabricated using the abovementioned monopole antennas. In particular, the wearable prototype is composed of a 16-element antenna array, embedded in a bra. The antennas are distributed asymmetrically around the bra surface, to reduce imaging artifacts that can be induced by a symmetric array. The antennas are located such that they are on the inside of the bra and will thus contact the skin when the bra is worn. This arrangement removes any uncertainty regarding the breast position relative to the array, i.e., the skin surface location is known. The antenna connectors protrude out of the bra, where they are connected to cables that are in turn connected to the

switching matrix and system that we have used previously. Note that at the current stage, only one cup of the bra has an integrated array, and as such all breast scans are performed only on this breast (i.e. the right one). In the future, the prototype will be updated to be able to accommodate both breasts.

Photographs of the antenna and the array from the table-based prototype are shown in Fig. 2, and the flexible array within the wearable prototype is shown in Fig. 3. In comparing the photographs, it is clear that the wearable prototype array has enabled a more compact patient interface, and that it will also provide a better fit to the breast.
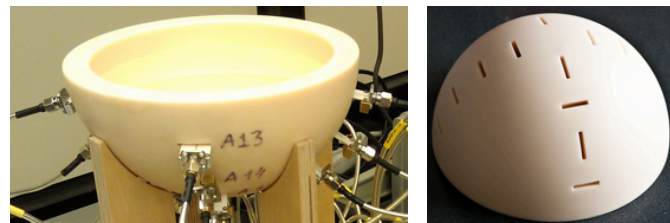

Fig. 2. Components of the table-based prototype. (Left) Antenna array and radome; (right) bottom view of radome with antenna slots visible.
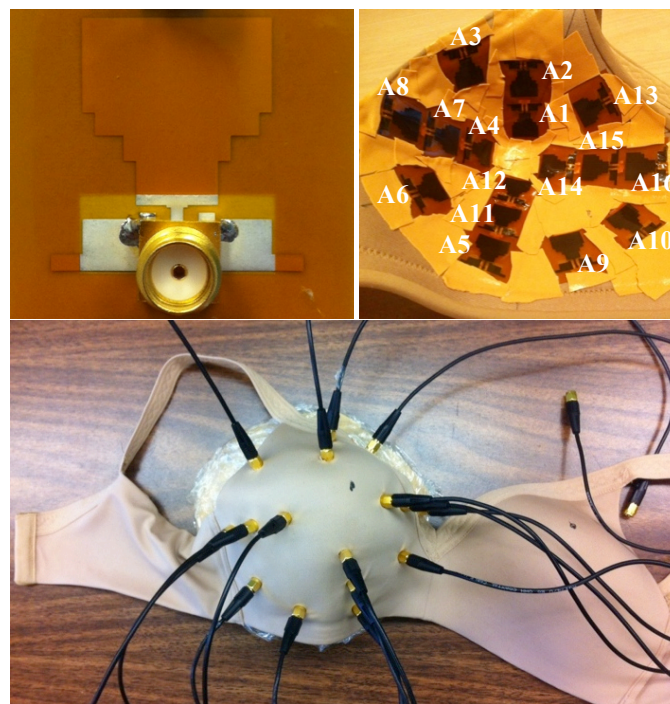
Fig. 3. The wearable prototype. Top, left: Close-up photograph of the connectorized monopole antenna, measuring 20×20 mm^2; top, right: photograph of the antenna array inside the bra-cup, with antenna numbers marked; bottom: photograph of the outside of the bra showing the SMA cables that connect to the antennas (the bra is sitting on a breast model).

The wearable prototype was designed at this stage to fit a specific volunteer. The volunteer's self-reported bra size is 38C. We have selected a bra with a size label of 36C for the prototype, with a cup smaller than the volunteer's typically worn size. This distinction is intentional: the slightly smaller bra ensures that the breast fills the bra entirely, and that the

antennas are being pushed against the skin. Even though it was sized down, the bra was still comfortable and easy to fit. We note that bra sizes are not standardized and tend to vary between manufacturer and country, so the label size alone should not be relied on and the bra must be verified to be a good fit prior to application.

Each antenna position is recorded in rectangular coordinates with respect to an origin in the bottom left-hand corner of the bra (as seen when facing the volunteer), at the location where that corner touches the skin. The coronal plane is the x-y plane, while the height from the chest wall to the nipple is denoted as the z-axis. The array positions in the coronal plane are plotted in Fig. 4, with each antenna labeled for clarity. Also shown in Fig. 4 is the "center" of the bra, where the peak occurs when travelling from the halfway point along the x-axis upwards in y, or from the halfway point in y upwards in x. This center location is presumably the place where the nipple is intended to rest. When fitting the volunteer, we discovered that, due to the unique anatomy of each individual, her nipple position was slightly off from the bra center – this position is also denoted in Fig. 4.
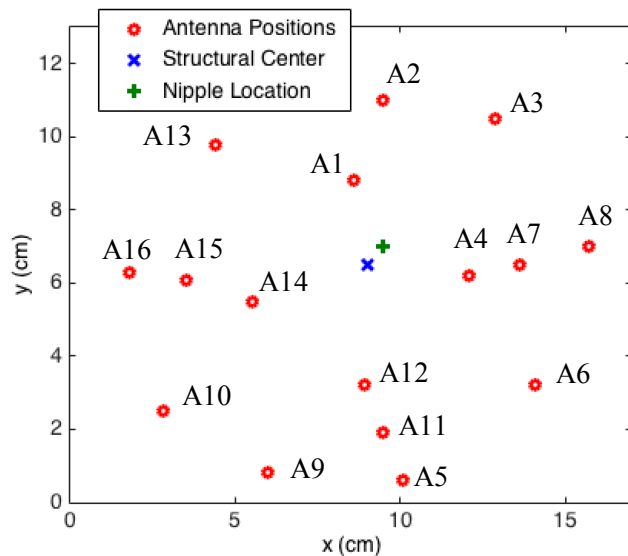

Fig. 4. Positioning for the array within the bra, top view when facing the volunteer. The antenna locations (projected on the x-y plane) are marked as red circles and are labeled numerically to identify each antenna. The bra center (i.e., where the material peaks furthest from the chest wall region) is labeled as a blue 'x'; and the nipple location for this specific volunteer (where the repositioning marker is) is shown as a green cross.

III. METHODOLOGY

In this work, we use a month-long measurement period as the basis for our investigation. We perform daily measurements on a healthy volunteer over the course of one menstrual cycle in order to verify the repeatability of measurements and to quantify the level of variation that the microwave system records in response to healthy tissue fluctuations. We conducted daily measurements on the volunteer with the table-based prototype, and now, in this work, we present a comparison study of measurements on the same volunteer with the wearable prototype.

A. Volunteer Description

The volunteer who participated in this study is a healthy 45-year old woman. She has no history of breast cancer, and her last mammogram (performed after the end date of this study) confirmed her healthy status. The volunteer has a cup size of C, enabling a good fit in both the dielectric radome of the table-based prototype and the wearable prototype. All components of this clinical study were approved by the Research Ethics Office at McGill University.

B. Measurements with Table-Based Prototype

With the table-based prototype, we conducted 27 breast scans over a 28-day period on the volunteer. This study was presented in [10], and found that daily relative permittivity estimates with this microwave system were in line with expected tissue changes over the course of a menstrual cycle as demonstrated in the literature [10]. With the table-based prototype, it was challenging to reposition the breast in the same way each day (with the same distribution of ultrasound gel around it) and thus the accuracy of relative permittivity estimates was not optimal. Further, this study found that imaging of a phantom in the same manner (with daily repositioning and an ultrasound immersion) over a one-month period led to highly consistent results, which demonstrated the repeatability of the system when no dielectric property changes were occurring. In this work, we also present measurements on the radome filled entirely with the immersion medium in order to emphasize the accuracy in relative permittivity estimates.

C. Wearable Prototype

For this series of tests, the wearable prototype was fixed in place such that neither the bra nor the cabling moved between measurements. Prior to a breast scan, the volunteer slips her arms through the straps of the wearable prototype, and then the straps are clasped at the back. In this way, the volunteer is secured in the bra. While putting the bra on, the nipple is aligned with a marker on the bra. This helps to further ensure that with the bra worn in this way, there is little space for repositioning error. As mentioned in the previous section, the breast contacts the antenna array directly, without an immersion medium. The snug fit of the array ensures good contact between the antennas and the skin, and a visual inspection of both the fit and the collected signals confirms this (without a good fit, air pockets may be present in the vicinity of the antenna, resulting in a noisy, low-amplitude signal). A poor connection is hence easy to detect. Analysis of the contact quality may be automated in future work.

In Fig. 5, two photographs (without and with cables attached) show the wearable prototype worn by the volunteer. These demonstrate that: a) the breast completely fills the bra and b) at all of the antenna locations the bra is slightly pushing into the skin, such that there is good contact between the antennas and the body. However, the cables will typically be connected when the bra is fitted. This is shown in the second picture of Fig. 5.

In this study, daily measurements were taken on the right breast of the volunteer, over a 28-day period. We note that the

volunteer's menstrual cycle has a consistent length of 28 days; however, the start day of the measurements did not coincide with the start of the follicular phase of the volunteer's cycle. In the following text, "Day1" denotes the first measurement day. We further note that measurements with the table-based prototype and the wearable prototype both started on the same day with respect to the cycle.
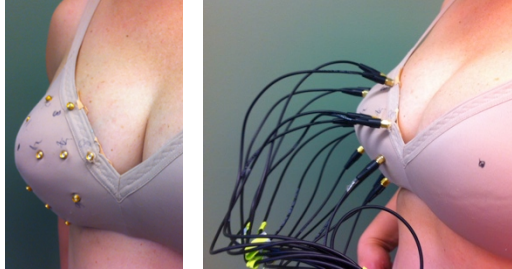

Fig. 5. The wearable prototype fitted to a volunteer: left picture, without cables; right picture, with cables.

The measurement and recording parameters were held constant during the study. The clock was fixed at 1 MHz, setting the pulse repetition rate. The oscilloscope sampled data at 160 GSa/s, for a total of 4096 samples per signal. With 16 antennas, there were a total of 240 signals collected per scan. Each collected signal was averaged 16 times to reduce the effects of random measurement noise. Each breast scan took approximately 6 minutes to complete.

We also recorded signals with the antenna array in contact with a phantom material (fat-mimicking, ε_r = 9.9 at centre frequency). As for the scan on ultrasound gel with the table-based prototype, this data was collected in order to verify the relative permittivity estimations obtained with the wearable prototype in a scenario that has less uncertainties than volunteer breast scans.

IV. SIGNAL ANALYSIS AND RESULTS

In this section, the data is examined directly based on the collected signals. First, we compare the received signal amplitudes from all transmit-receive antenna pairs of the table-based prototype and the wearable prototype. The data sets are obtained from breast scans of the right breast of the same volunteer. For all scans with both prototypes, the signal amplitude fed into the transmit antenna was constant. A summary chart is presented in Table I, where the number of antenna pairs that result in collected signals above three threshold values (250 mV, 200 mV, and 100 mV) is listed. These particular threshold values are chosen arbitrarily as an example. High-amplitude signals can be used as an indicator of the system performance: with the same input signal, higher outputs represent lower overall path losses (due to any or all of: less attenuation, fewer interfaces for scattering, improved matching, better antenna efficiency, etc.). As can be seen from Table I, the wearable prototype leads to more antenna pairs with high amplitude signals for all three thresholds. Further, over all antenna pairs, the wearable prototype signals are on average 10% stronger in amplitude than the table-based

prototype signals. This suggests that the elimination of the ceramic radome and the immersion medium in the wearable prototype has indeed helped to reduce loss. Further, the transmission path lengths are now shorter as the antennas contact the skin directly and thus the path is comprised only of the travel through the breast. In particular, there are less interfaces involved with the wearable prototype, and thus fewer reflections to attenuate the signal of interest: with the table-based prototype, the signal contains responses from the antenna-radome interface, the radome-ultrasound gel interface, the ultrasound gel-skin interface, and from interior tissues. For the wearable prototype, the main responses that contribute to the signals are limited to the reflection from the antenna-skin interface and reflections from the interior tissues.

In Table I, we also present the numbers of signals that are at or below the noise threshold for measurements on this specific volunteer with both prototypes. In general, the system noise floor is at -80 dB (relative to the input); however, the received signal noise level will change depending on breast heterogeneity, with more heterogeneous breasts resulting in more clutter that contributes noise to the signals. Thus, the effective noise floor for signals with this patient is just below -60 dB. From Table I, it is noted that with the table-based prototype, 16 signals (1/15th of the data set) are near or below the noise level for breast scans with that volunteer and prototype. For the wearable prototype, with the same volunteer, all signals are above the noise level. This result may have an impact on the ability of the system to detect malignancies: with fewer collected signals near the noise floor, more signals can then contribute useful information to tumor detection or imaging algorithms.

TABLE I.
COMPARISON OF THE NUMBER OF ANTENNA PAIRS RECORDING HIGH-AMPLITUDE SIGNALS AND ANTENNA PAIRS WITH AMPLITUDE AT OR BELOW NOISE LEVEL, FOR THE TABLE-BASED AND WEARABLE PROTOTYPES: THE NUMBER OF TRANSMIT-RECEIVE ANTENNA PAIRS WITH PEAK RECEIVED SIGNAL AMPLITUDE ABOVE 250 MV, 200 MV, AND 100 MV, AND BELOW THE NOISE LEVEL.

	> 250 mV	> 200 mV	> 100 mV	≤ Noise
Table-Based	6	16	48	16
Wearable	8	23	51	0

Next, the collected signals are processed in order to estimate the average relative permittivity, ε_r, of the breast for each day, and for the known materials (ultrasound gel for the table-based prototype and a fat-mimicking material for the wearable prototype). The relative permittivity estimate is based on the difference in travel time of the wave between various antenna pairs. For the wearable prototype, the antennas are positioned at known locations in contact with the breast surface, thus the distance between antennas, and therefore the distance travelled within the breast tissue, is also known. Comparing the signal arrival times of two select antenna pairs then provides all of the information necessary to estimate the relative permittivity, as follows:

$$\varepsilon_r = \left(c \, \frac{\Delta t}{\Delta d} \right)^2 \qquad (1)$$

where c is the speed of light in a vacuum, Δt is the difference in signal arrival time between two antenna pairs, and Δd is the difference in distance travelled for a wave passing between the two antenna pairs. The difference is calculated from the known three-dimensional antenna coordinates. We note that the signals for each antenna pair are taken from the same day's scan.

This method of estimation was confirmed through testing on measurements obtained when scanning the region filled entirely with a medium of known dielectric properties. For the table-based prototype, the radome was filled entirely with ultrasound gel ($\varepsilon_r = 68$ at 3 GHz), and full scans were performed. The mean relative permittivity calculated was 66.92, an error of 1.6% from the expected value (68). For the wearable prototype, a more realistic material, the fat-mimicking material, was scanned, resulting in a mean estimated relative permittivity of 9.88, with an error of 0.2% from the known value (9.9). These results indicate that the prototypes are able to provide relative permittivity estimates that are in-line with the actual permittivity values of the material under test.

In Fig. 6, the estimated relative permittivity of the volunteer's breast is plotted for each day of the study. The data obtained with the wearable prototype is also compared to that from the table-based prototype, initially presented in [10]. The relative permittivity estimate is affected by jitter, for which we have compensated, but it cannot be eliminated completely. Jitter is compensated for by aligning the signals in the time-domain using a cross-correlation method. We have further reduced the jitter contribution by taking estimates from two sets of antenna pairs (A3A5 and A16A6, plus A5A3 and A6A16) and averaging the results. These antenna pairs were chosen as they represent scenarios in which the signal has passed through the breast (as opposed to being reflected off of it); any pair that represents such a transmission scenario could likewise be used in this calculation. Any residual effects of jitter appear in the relative permittivity values randomly. A further small source of error is the antenna positions, which are accurate only down to 1 mm. In the ε_r estimate, the imprecision in the antenna location shows up as an offset error – as each day's measurement is affected systematically in the same way.

An overview of the data plotted in Fig. 6 is provided in Table II. For both the table-based prototype and the wearable prototype, the mean relative permittivity is shown, along with the standard deviation and range, across all measurement days. With the wearable prototype, both the standard deviation and range of ε_r are decreased relative to the table-based prototype. This suggests that the wearable prototype has succeeded in diminishing uncertainties found in the table-based prototype, for instance due to improvement in fixed positioning of the breast. The decrease in standard deviation of relative permittivity could also be attributed to the stronger signal levels collected with the wearable prototype, enabling a higher signal-to-noise ratio.

Another notable feature of the relative permittivity data from Fig. 6 is that with the wearable prototype the mean over

the month is 23.3, whereas with the table-based prototype it was 27.9. We believe that this can be attributed to an unavoidable source of error in the relative permittivity calculations for the table-based prototype, that does not exist with the wearable prototype. More specifically, with the table-based prototype, we had to account for the immersion medium between the radome and the breast in order to extract only the breast's estimated relative permittivity. However, the exact thickness and distribution of the immersion medium was difficult to estimate, and varied between antenna pairs. This led to an offset error in the relative permittivity estimates that was approximately constant over all days. Based on the fact that the relative permittivity estimate was on average higher with the table-based prototype, an under-estimate in the thickness of the immersion medium may have occurred. As the immersion medium was ultrasound gel, under-estimating its thickness would lead to an increase in the estimated tissue properties (the gel relative permittivity is higher than tissue properties), as is seen in Fig. 6. For all of these reasons, we can confidently conclude that the estimated relative permittivity for the wearable prototype is more reliable than that of the table-based prototype.
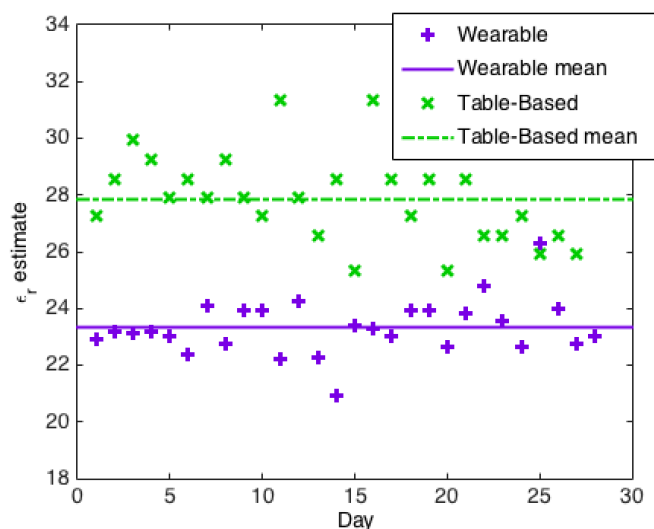

Fig. 6. Estimated relative permittivity (εr) for each day for data collected from the patient with the table-based prototype (from [10]) and the wearable prototype.

TABLE II.
STATISTICS ON AVERAGE BREAST RELATIVE PERMITTIVY ESTIMATE FOR BOTH PROTOTYPES.

	Table-Based	Wearable
Mean	27.9	23.3
Standard Deviation	1.60	0.98
Range	6.0	5.3

The relative permittivity values estimated for both prototypes correspond to the BI-RADS breast density classification of the volunteer (class II). This level of tissue density is suggestive of scattered fibroglandular tissue. A further takeaway from these results is the range of expected

breast tissue changes (as perceived by the microwave system) throughout the course of a menstrual cycle. The studies in [14] and [15] show that, for patients in the age group of our volunteer, breast tissues may be, on average, more dense during the luteal phase than during the follicular phase of the menstrual cycle. With the wearable prototype, the average ε_r over the first 14 measurement days is 23.0, while the average over days 15 to 28 is 23.7. This difference falls within the standard deviation of measurements and it is not possible to conclude that it is not due to uncertainties in the estimates. Despite this, the results are consistent with those found in the literature. The collected data can be used to obtain the expected level of tissue changes seen by the microwave imaging technique due to variations that are attributed to healthy (non-cancerous) causes, for this specific volunteer. Further investigations may aim to collect similar data from a large sample of volunteers, in order to characterize and differentiate, if possible, the size of variations due to healthy tissue changes and due to growth of malignancies.

V.   IMAGING ANALYSIS AND RESULTS

In this section, the collected volunteer data is processed to generate images and these are subsequently subjected to analysis. In particular, the breast scan data from each of the 28 measurement days is used to reconstruct images of the scattering within the breast tissues. Prior to inputting the data into an imaging algorithm, each signal is filtered to remove content outside of the frequency range of the transmitted pulse using a low-pass filter with a cutoff at the upper limit of the frequency range of interest. Jitter is compensated for by time aligning the data using the correlation alignment method presented in [16]. The algorithm used is the Delay-Multiply-and-Sum (DMAS) method [17]. The average tissue properties obtained in Section IV are used in the image formation process.

With the DMAS algorithm, as is typical with radar techniques, the reconstructed image highlights regions of electromagnetic scattering, rather than recovering the dielectric property profile. Fig. 7 shows a sample of the reconstructed images, for volunteer data obtained with the wearable prototype, from Days 7, 15, and 21 of the 28-day measurement period. The images shown are 2-D coronal slices of a full 3-D image, each at the same depth (6 mm from the chest wall, toward the nipple). Each image is normalized to the maximum pixel intensity over the 3-D space of the entire image. As they have been normalized, the resulting color scale is unitless; red regions represent areas of scattering, while blue indicates regions of little or no scattering. Since the volunteer is healthy, the red regions indicate denser tissue regions. The image color scale is linear.

From Fig. 7, it is evident that the images show consistency in the recordings over the measurement days. By purely visual examination, it is difficult to identify changes in the images between days. These results emphasize that the antenna-breast contact is consistent over scan days, as the images demonstrate highly repeatable data each time the volunteer
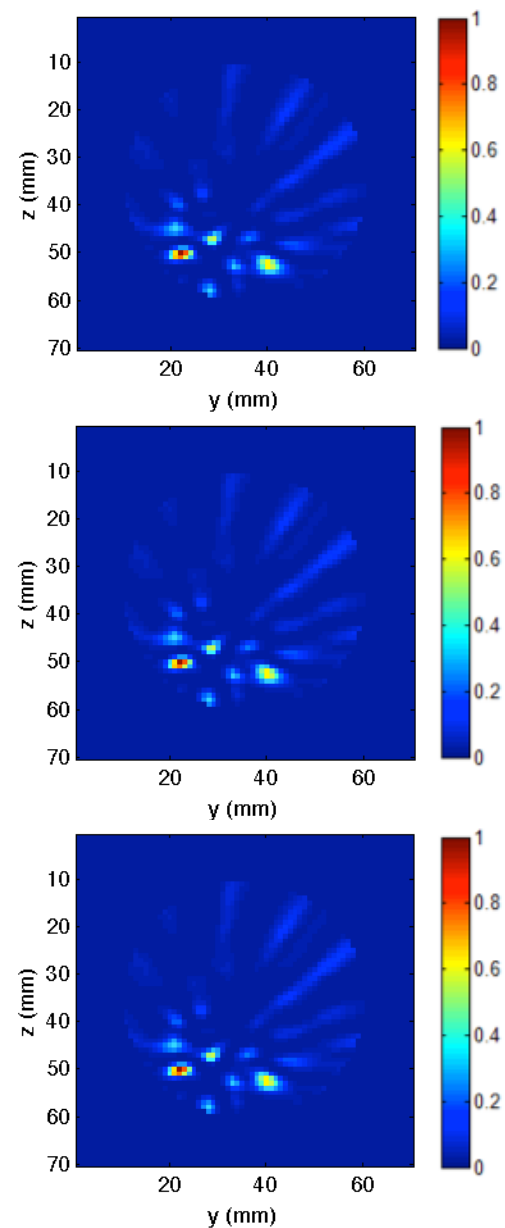

Fig. 7. Reconstructed images for a slice taken at a depth of 6 mm from the chest wall, from top to bottom: from Day 7, from Day 15, and from Day 21.

puts on the wearable prototype. To gain a more in-depth understanding of the image data, we use a similarity metric to compare the images over the days of the month-long measurement period. Such metrics are used to assess how similar two images are to each other. Common methods include cross-correlation and mean square error (MSE) [18], [19], both of which compare images based on their pixel intensities, on a pixel-to-pixel basis. We use another type of method that compares the relationships between the pixels, or, in other words, the structural content of the images. In particular, we have chosen to use the Structural Similarity Index (SSIM, for **S**tructural **Sim**ilarity) [20]. This metric considers three image characteristics: the luminance, the contrast, and the structure. First, the luminance and contrast are compensated for so that the two images under

consideration are on the same scale. Then, these normalized images are compared based on their structure. The SSIM provides a value of one if the two images are identical to each other, and a value of zero if they have no similarity whatsoever.

The SSIM operates on 2-D images. As our reconstruction of the breast is 3-D, we obtain SSIM values by calculating a value for each 2-D slice, then averaging over all slices for a final value for each 3-D image. In Fig. 8, the SSIM is shown for each day of measurements, in which the image from Day X $\{X=2{:}28\}$ is compared to the image from Day 1. The data shown in orange (diamonds) corresponds to the breast scans collected with the wearable prototype. For comparison purposes, this is plotted against the data obtained with the table-based prototype with the volunteer, and phantom data from both prototypes.
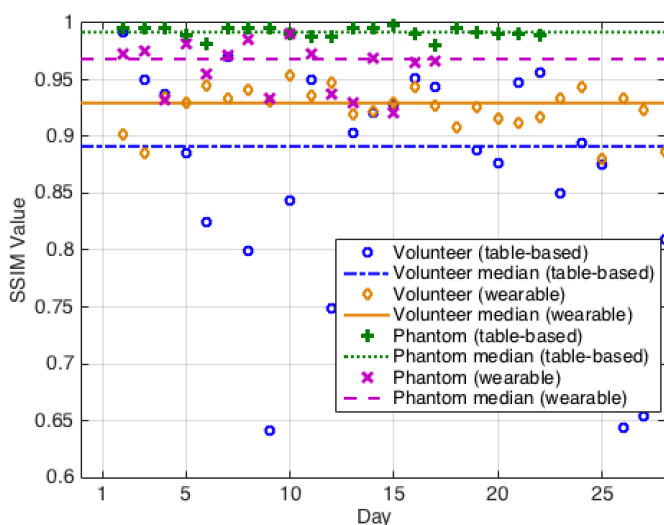

Fig. 8. SSIM values for images from all days compared to the image from Day 1: with the table-based prototype with ceramic dielectric radome, volunteer data (blue, circles) and phantom data (green, crosses) [10]; with the wearable prototype, volunteer data (orange, diamonds) and phantom data (purple, x's). Volunteer data is from the right breast (same volunteer for all measurements).

Table III summarizes the SSIM value statistics for the wearable prototype, and the table-based prototype. From Fig. 8 and Table III, it is evident that for the volunteer the wearable prototype produces images that are more repeatable than those of the table-based prototype. The images obtained from volunteer scans with the wearable system lead to a mean SSIM of 0.925 over the 28-day period, whereas the same volunteer scans with the table-based prototype had a mean of 0.869. We believe that we can attribute this improvement to the fact that with the wearable prototype, the breast position is more fixed and known, due to the lack of immersion medium and the use of a breast-fitting radome. The standard deviation and range of SSIM values are also lower for the wearable prototype than with the table-based prototype. This result confirms that the wearable prototype works at least as well as the table-based prototype, for this volunteer.

We note that the phantom measurements with the table-based prototype have a mean SSIM of 0.992, while the

wearable prototype phantom measurements have a mean of 0.960. The higher SSIM with the table-based prototype is due to the fact that the phantom shape (rigid hemisphere) is designed to fit the table-based radome, and as a result the wearable prototype does not conform as well to the phantom as it does to the breast. In general, phantom measurements with both prototypes have higher SSIM than volunteer measurements. This is attributed to two factors: i) the phantom used was stable in dielectric properties over the measurement period, and ii) repositioning of the phantom is easier to control than repositioning of a person. As the wearable prototype diminishes the significant question of breast position, the residual differences in SSIM over the days are suggestive of breast tissue changes in accordance with the menstrual cycle.

TABLE III.
SSIM STATISTICS FOR DATA FROM TABLE-BASED AND WEARABLE PROTOTYPES (WITH PHANTOM AND VOLUNTEER).

	Table-Based		Wearable	
	Phantom	*Volunteer*	*Phantom*	*Volunteer*
Mean	0.992	0.869	0.960	0.925
Standard Deviation	0.005	0.101	0.022	0.019
Range	0.018	0.350	0.071	0.073

In general, the SSIM metric can be used to quantify the level of change occurring in tissue between breast scans, the interpretation of which may suggest that changes are limited to healthy variations or that they indicate abnormalities. As an example, if a healthy patient is scanned repeatedly over two years and the corresponding SSIM is always between [0.89, 0.93], then a new scan with a value of 0.86 would be suggestive of an unusual level of breast tissue changes (possible tumor growth). However, equally, a patient could have typical healthy measurements with SSIM varying between [0.80, 0.93], and in this case a new scan resulting in an SSIM value of 0.86 would not be remarkable. Thus, the implications of the SSIM values are best interpreted on a patient-basis and are not absolute indicators of breast health.

Lastly, we briefly discuss the cost of the wearable prototype relative to the table-based prototype. From the table-based prototype, three main components have been replaced in the wearable bra: the ceramic radome, the antennas, and the immersion medium. The ceramic radome cost approximately $3000 (all amounts in CAD) to fabricate, and the original 16 antennas were fabricated by hand, taking approximately 40 hours of work with a total fee of $1300. In contrast, the 'radome' for the wearable prototype (the bra) was obtained for less than $20. The antennas were printed, allowing for a significant decrease in man-hours and cost (~$10/antenna). Use of the immersion medium cost only a few dollars per breast scan, but it must be replaced in between patients and thus costs add over time. The immersion cost is removed completely with the wearable prototype. Overall, the wearable prototype is a significant improvement in terms of lowering the cost of such a device.

VI. CONCLUSION

This work has introduced a clinical prototype for time-domain microwave breast cancer detection. The prototype has a wearable interface, i.e., a bra that contains the antenna array. The wearable prototype is worn with the antennas directly contacting the skin, eliminating the need for a messy immersion medium, and giving precise knowledge of the position of the breast surface relative to the array. The system-breast interface of the wearable prototype is highly cost-effective compared to typical table-based microwave breast imaging systems. We have performed breast scans with the wearable prototype on a healthy volunteer, and compared the resulting data to that collected with our table-based prototype. Signal and image analysis have both demonstrated that the wearable prototype is an improvement over the table-based prototype. Further, the daily measurements, spanning over a single menstrual cycle, provided a baseline for healthy tissue variation, as perceived by the microwave prototype; data that is key for a breast health monitoring application.

Future work, along the direction of system improvement, includes integration of other hardware components, a bra with a wider coverage area and reduced scanning time. Further, we will expand clinical testing to a wider range of healthy volunteers (with varying breast size and density) as well as breast cancer patients.

REFERENCES

[1]   M. Lazebnik, et al., "A large-scale study of the ultrawideband microwave dielectric properties of normal, benign and malignant breast tissues obtained from cancer surgeries," *Phys. Med. Biol.*, vol. 52, no. 20, pp. 6093–6115, 2007.

[2]   N. Nikolova, "Microwave Biomedical Imaging," J. Webster (ed.), Wiley Encyclopedia of Electrical and Electronics Engineering, John Wiley & Sons, Inc., pp. 1–22, 2014.

[3]   X. Zeng, A. Fhager, P. Linner, M. Persson, and H. Zirath, "Experimental Investigation of the Accuracy of an Ultrawideband Time-Domain Microwave-Tomographic System," *IEEE Trans. Instrum. Meas.*, vol. 60, no. 12, pp. 3939–3949, Dec. 2011.

[4]   M. Klemm, I. J. Craddock, J. A. Leendertz, A. Preece, D. R. Gibbins, M. Shere, and R. Benjamin, "Clinical trials of a UWB imaging radar for breast cancer," in *Proc. Eur. Conf. Antennas and Propagation (EuCAP)*, Barcelona, Spain, Apr. 12–16, 2010.

[5]   J. Bourqui, J. M. Sill, and E. C. Fear, "A prototype system for measuring microwave frequency reflections from the breast," *Int. J. Biomed. Imaging*, vol. 2012, Article ID 851234, pp. 1–12, 2012.

[6]   J. Bourqui, J. Garrett, and E. C. Fear, "Measurement and Analysis of Microwave Frequency Signals Transmitted through the Breast," *Int. J. Biomed. Imaging*, vol. 2012, Article ID 562563, pp. 1–11, 2012.

[7]   E. C. Fear, et al., "Microwave Breast Imaging With a Monostatic Radar-Based System: A Study of Application to Patients," *IEEE Trans. Microw. Theory Techn.*, vol. 61, no. 5, pp. 2119–2128, 2013.

[8]   P. M. Meaney, et al., "Microwave imaging for neoadjuvant chemotherapy monitoring: initial clinical experience," *Breast Cancer Research*, vol. 15, no. 2, pp. 1–16, 2013.

[9]   E. Porter, E. Kirshin, A. Santorelli, M. Coates, and M. Popović, "Time-domain multistatic radar system for microwave breast screening," *IEEE Antennas Wireless Propag. Lett.*, vol. 12, pp. 229–232, 2013.

[10]   E. Porter, A. Santorelli, R. Kazemi, and M. Popović, "Microwave Time-Domain Radar: Healthy Tissue Variations Over the Menstrual Cycle," *IEEE Antennas Wireless Propag. Lett.*, vol. PP, no. 99, pp. 1–4, 2015.

[11]   H. Kanj, and M. Popović, "A novel ultra-compact broadband antenna for microwave breast tumor detection," *Prog. Electromagn. Res.,* vol. 86, pp. 169–198, 2008.

[12]   H. Bahrami, E. Porter, A. Santorelli, B. Gosselin, M. Popović, and L. A. Rusch, "Flexible Sixteen Antenna Array for Microwave Breast Cancer Detection," *IEEE Trans. Biomed. Eng.*, vol. 62, no. 10, pp. 2516 - 2525, 2015.

[13]   H. Bahrami, E. Porter, A. Santorelli, B. Gosselin, M. Popović, L. A. Rusch, "Flexible sixteen monopole antenna array for microwave breast cancer detection," in *Proc. Eng. Med. Biol. Soc. (EMBC), 36th Ann. Intl. Conf. IEEE*, pp. 3775-3778, Aug. 26-30, 2014.

[14]   G. Ursin, et al., "Mammographic Density Changes During the Menstrual Cycle," *Cancer Epidemiol. Biomarkers Prev.*, vol. 10, pp. 141–142, 2001.

[15]   E. White, et al, "Variation in mammographic breast density by time in menstrual cycle among women aged 40-49 years," *J. Natl. Cancer Inst.*, vol. 90, no. 12, pp. 906–910, 1998.

[16]   E. Porter, E. Kirshin, A. Santorelli, and M. Popović, "Microwave Breast Screening in the Time-Domain: Identification and Compensation of Measurement-Induced Uncertainties," *Prog. Electromagn. Res. B*, vol. 55, pp. 115–130, 2013.

[17]   H. B. Lim, N. T. T. Nhung, E. P. Li, and N. D. Thang, "Confocal microwave imaging for breast cancer detection: Delay-multiply-and-sum image reconstruction algorithm," *IEEE Trans. Biomed. Eng.*, vol. 55, no. 6, pp. 1697–1704, Jun. 2008.

[18]   V. Di Gesù, and V. Starovoitov, "Distance-based functions for image comparison," *Pattern Recognition Lett.*, vol. 20, pp. 207–214, 1999.

[19]   G. Penney, J. Weese, J. A. Little, P. Desmedt, D. L. G. Hill, D. J. Hawkes, "A Comparison of Similarity Measures for Use in 2-D – 3-D Medical Image Registration," *IEEE Trans. Med. Imag.*, vol. 17, no. 4, pp. 586–595. Aug. 1998.

[20]   Z. Wang, A. C. Bovik, H. R. Sheikhm and E. P. Simoncelli, "Image quality assessment: From error visibility to structural similarity," *IEEE Trans. Image Process.,* vol. 13, no. 4, pp. 600–612, Apr. 2004.